Estimation of biogenic VOC emissions and their corresponding impact on ozone and secondary organic aerosol formation in China

Kai Wu, Xianyu Yang, Dean Chen, Shan Gu, Yaqiong Lu, Qi Jiang, Kun Wang, Yihan Ou, Yan Qian, Ping Shao, Shihua Lu

PII: S0169-8095(19)30471-5
DOI: https://doi.org/10.1016/j.atmosres.2019.104656
Article Number: 104656
Reference: ATMOS 104656

To appear in: *Atmospheric Research*

Received date: 17 April 2019
Revised date: 19 July 2019
Accepted date: 22 August 2019

Please cite this article as: K. Wu, X. Yang, D. Chen, et al., Estimation of biogenic VOC emissions and their corresponding impact on ozone and secondary organic aerosol formation in China, Atmospheric Research, https://doi.org/10.1016/j.atmosres.2019.104656

Estimation of biogenic VOC emissions and their corresponding impact on ozone and secondary organic aerosol formation in China

Kai Wu[1], Xianyu Yang[1,*] xyang@cuit.edu.cn, Dean Chen[2], Shan Gu[1], Yaqiong Lu[3], Qi Jiang[1], Kun Wang[4], Yihan Ou[1], Yan Qian[5], Ping Shao[1], Shihua Lu[1]

[1]Plateau Atmosphere and Environment Key Laboratory of Sichuan Province, School of Atmospheric Sciences, Chengdu University of Information Technology, Chengdu 610225, China

[2]Institute for Atmospheric and Earth System Research (INAR)/Physics, Faculty of Science, University of Helsinki, Helsinki 00560, Finland

[3]Institute of Mountain Hazards and Environment, Chinese Academy of Sciences, Chengdu 610041, China

[4]Department of Air Pollution Control, Beijing Municipal Institute of Labor Protection, Beijing 100054, China

[5]State Key Laboratory of Environmental Criteria and Risk Assessment & Environmental Standards Institute, Chinese Research Academy of Environmental Sciences, Beijing 100012, China

[*]Corresponding author at: Plateau Atmosphere and Environment Key Laboratory of Sichuan Province, School of Atmospheric Sciences, Chengdu University of Information Technology, Chengdu 610225, China.

Abstract

Biogenic volatile organic compounds (BVOC) play an important role in global environmental chemistry and climate. In the present work, biogenic emissions from China in 2017 were estimated based on the Model of Emissions of Gases and Aerosols from Nature (MEGAN). The effects of BVOC emissions on ozone and secondary organic aerosol (SOA) formation were

investigated using the WRF-CMAQ modeling system. Three parallel scenarios were developed to assess the impact of BVOC emissions on China's ozone and SOA formation in July 2017. Biogenic emissions were estimated at 23.54 Tg/yr, with a peak in the summer and decreasing from southern to northern China. The high BVOC emissions across eastern and southwestern China increased the surface ozone levels, particularly in the BTH (Beijing-Tianjin-Hebei), SCB (Sichuan Basin), YRD (Yangtze River Delta) and central PRD (Pearl River Delta) regions, with increases of up to 47 μg m^{-3} due to the sensitivity of VOC-limited urban areas. In summer, most SOA concentrations formed over China are from biogenic sources (national average of 70%). And SOA concentrations in YRD and SCB regions are generally higher than other regions. Excluding anthropogenic emissions while keeping biogenic emissions unchanged results that SOA concentrations reduce by 60% over China, which indicates that anthropogenic emissions can interact with biogenic emissions then facilitate biogenic SOA formation. It is suggested that controlling anthropogenic emissions would result in reduction of both anthropogenic and biogenic SOA.

Keywords: BVOC, Ozone, Modeling, MEGAN, SOA

1 Introduction

Biogenic volatile organic compounds (BVOCs) emitted from terrestrial ecosystems have substantial effects on the global climate and environmental chemistry. Previous studies have shown that up to 90% of the total VOC emissions are derived from biogenic sources (Guenther et al., 1995). BVOCs such as isoprene, monoterpenes and sesquiterpenes participate in oxidative chemical reactions in the atmosphere with oxidants such as ozone, OH and NO_3 radicals. In addition, BVOCs are major sources of secondary organic aerosols (SOA) and new particle formation (Hallquist et al., 2009; Kulmala et al., 2004; Paasonen et al., 2013; Kota et al., 2015).

Measurements and modeling of BVOC emissions are of vital importance to understand the carbon cycle, biosphere-atmosphere interactions and climate change (Gu et al., 2017; Hantson et al., 2017).

Over the past few decades, research has been focused on four objectives: (1) developing and improving BVOC instruments and technology, (2) quantifying the effects of BVOC emissions, (3) developing and improving BVOC emission models, and (4) understanding the mechanisms underlying the interactions of BVOCs with anthropogenic volatile organic compounds (AVOCs). Most BVOCs are highly reactive and readily interact with oxidants, consequently influencing the atmospheric composition. Therefore, accurately estimating the BVOC emissions can improve the results of studies of the effects of BVOCs on the regional and global air quality and climate systems (Makkonen et al., 2012).

BVOC emissions are calculated with models, and the Model of Emissions of Gases and Aerosols from Nature (MEGAN) is one of the models commonly used (Guenther et al., 2006). The standard emission potential of a plant depends on the plant functional type (PFT) and its biomass. Moreover, the driving factors of emission activities are the PFT type, leaf area index (LAI), temperature, radiation, wind speed, humidity and soil moisture content. The meteorological variables can be obtained from observations, reanalysis data and weather forecasting models, and the PFT type, biomass and LAI are obtained from remote sensing databases.

BVOC emissions have been studied regionally and globally for the past several decades (Graedel et al., 1993). Global emissions of biogenic isoprene and monoterpenes were estimated to be 400-600 Tg/yr and 33-147 Tg/yr, respectively (Arneth et al., 2011). In China, BVOC emissions from plants are estimated to be approximately 1.5 times those from anthropogenic

sources. And several studies have been conducted for analyzing the characteristics of BVOC emission in China. However, most studies mainly focused on local and regional scale for the Pearl River Delta (PRD), Beijing, Hong Kong, and Yangtze River Delta (YRD) regions based on various methodologies (Liu et al., 2018; Ou et al., 2015; Pan et al., 2015; Situ et al., 2013; Tsui et al., 2009). Furthermore, in the context of global warming, Fu and Liao (2012) reported that isoprene and monoterpene emissions in China displayed large interannual variations of 15-42% and 10-32% from 2001-2006, respectively. Li and Xie (2014) studied the changes in emissions in China from 1981-2003 and discovered an increase in BVOC emissions induced by a biomass increase. Due to the large interannual variations of BVOC emissions, it is expected that previous estimates of national BVOC emissions in China which concentrated on early time may not reflect their current characteristics. Therefore, updating BVOC emissions is necessary to provide scientific support for air quality improvements in China.

Modeling and laboratory studies have shown that BVOC emissions can affect surface ozone and SOA. With the remarkable economic development and rapid increase of fossil fuel consumption, the air quality in China has deteriorated in recent years. Ground-level ozone pollution has become a major air quality issue in China. In addition, heavy pollution episodes exceeding 120 ppbv often occur in metropolis clusters such as Beijing-Tianjin-Hebei, the Yangtze River Delta and Sichuan Basin. A better understanding of the causes of elevated ozone in China is critical to develop effective emissions control strategies. Biogenic SOA (BSOA) is a major pollutant worldwide. Because of the large anthropogenic emission sources in China, anthropogenic SOA could be comparable to BSOA. Ding et al. (2014) analyzed SOA tracers from isoprene, monoterpenes, sesquiterpene and aromatics in China and found that isoprene and aromatics are primary contributors to SOA. Mo et al. (2018) investigated the contribution of

biogenic isoprene emissions to ground-level ozone formation based on ground-based measurements in Beijing and found that isoprene emissions accounted for half of the total ozone formation potential. Qin et al. (2018) employed the CMAQ model to simulate isoprene-derived and monoterpene-derived BSOA formation in China, and the results indicated that isoprene-derived BSOA dominates BSOA formation in China. However, those studies focused only on a specific temporal period or regional scale. The overall impact of BVOC emissions on ground-level ozone and SOA formation in China remains unclear and must be addressed.

In this study, the objectives are to estimate BVOC emissions in China at a high spatial resolution and probe the effects of BVOC emissions on ground-level ozone and SOA formation in China. MEGAN version 2.1 and Weather Research and Forecasting model coupled with the Community Multiscale Air Quality (WRF-CMAQ model) were adopted to estimate BVOC emissions and investigate the impacts of BVOC emissions on ground-level ozone and SOA. The year 2017 was selected as the base year to simulate the spatiotemporal variations in BVOC emissions. The paper is organized as follows. Section 2 introduces the methodologies and databases used to estimate biogenic emissions, as well as the WRF-CMAQ framework. The model performance is described in Section 3, with comparisons of meteorological data on BVOC emissions with model results. Moreover, the effects of BVOC emissions on summertime O_3 and SOA formation are described in Section 3. The conclusions are presented in Section 4.

2 Methodology

2.1 WRF configuration

The WRF model version v3.9.1 was adopted to provide meteorological conditions for high spatiotemporal resolution data to determine the diurnal relative humidity, temperature, solar radiation, and wind speed. The spatial and temporal resolutions were 27 km × 27 km and 1 h,

respectively. The vertical dimensions were 27 levels with a 100 hPa model top. The initial and boundary conditions were obtained from the National Centers for Environmental Prediction (NCEP) FNL 1.0° × 1.0° reanalysis data (http://dss.ucar.edu/datasets/ds083.2/). To improve the model performance, the NCEP ADP Operational Global Surface Observations were used for surface reanalysis and four dimensional data assimilation. And we chose proper strength of nudging coefficients, i.e., 0.00001 sec^{-1} is used for nudging of water vapor mixing ratio and 0.00005 sec^{-1} is used for nudging of both u/v-wind potential temperature (Hogrefe et al., 2015; Xing et al., 2015; Xing et al., 2017). The components of the model setup are listed in Table 1.

Table 1. WRF analysis options.

Component	Option
Microphysics	Scheme of Lin et al.
Longwave radiation	RRTM scheme
Shortwave radiation	Goddard shortwave
Surface layer	MM5 similarity
Land surface	Noah Land Surface Model
Planetary boundary layer	Yonsei University scheme
Cumulus parameterization	Grell 3D

2.2 MEGAN configuration

MEGAN v2.1 (Guenther et al., 2012) was utilized to estimate BVOC emissions in China with a 27-km horizontal grid spacing domain (shown in Fig. 1). The inputs for MEGAN include the LAI, PFTs, emission factors, and meteorological data (e.g., solar radiation, temperature, relative humidity and soil moisture). The monthly average LAI was obtained from the 8-day MODIS LAI product (MOD15A2, 2017) with the same horizontal resolution as the study domain, as shown in Fig. 2. The PFT map was obtained from the MODIS MCD12Q1 product and regridded into the WRF domain to compute the fraction of each PFT in each grid. The default

MEGAN emission factors (mg m^{-2} h^{-1}) with a resolution of 30 s (~1 km), which reflect the BVOC emission rate under standard canopy conditions, were leveraged (http://lar.wsu.edu/megan/guides.html). Meteorological conditions were simulated by the WRF model. A one-year MEGAN simulation was performed for 2017 in China.

2.3 CMAQ configuration

We set up Community Multiscale Air Quality model (CMAQ version 5.2.1, Foroutan et al. (2017)) (https://www.cmascenter.org/cmaq/) to simulate the atmospheric composition over China with the same domain and grid resolution for WRF and MEGAN. The initial and boundary conditions for CMAQ simulation were based on the CMAQ default profiles which represent unpolluted atmosphere. The CB05 represented the gas phase, and AERO6 represented the aerosol chemical mechanisms (Appel et al., 2013). For the simulation of SOA, we used the default SOA module of the CMAQv5.2.1. It simulates NMVOC-derived SOA with a two-product model, treats primary organic aerosol (POA) as nonvolatile and nonreactive, and ignores IVOC emissions. Carlton et al. (2010) provided a detailed description of aerosol chemistry in CMAQ, including SOA formation from benzene, isoprene and sesquiterpenes. The POA oxidation mechanism is described in Simon & Bhave (2012). The new updates in CMAQ v5.2.1 accounts for the semivolatile partitioning and gas-phase aging of these POA compounds consistent with experimentally derived parameterizations (Murphy et al., 2017), SOA properties and IEPOX organosulfate formation rate constant were updated (Pye et al., 2017). We selected July as representative of summertime and acquired anthropogenic emissions for the CMAQ domain from the MEIC emission inventory 2016 developed by Tsinghua University (http://www.meicmodel.org/), which contains monthly gridded (0.25° × 0.25°) emissions

information for anthropogenic emissions in the CB05 mechanism. The biogenic emissions were modeled using MEGAN (described in Section 2.2).

3 Results and discussion

3.1 Evaluation of the performance of the WRF model and MEGAN

Fig S1 and S2 show the seasonal spatial distribution of temperature at 2m (T2) and the daily downward shortwave radiation (DSW) simulated by the WRF model. And these meteorological factors were evaluated using in situ measurement data from 824 and 84 national meteorological sites, respectively. The in situ measurement data are from the China Meteorological Data Sharing Service System (http://data.cma.cn/). Table 2 presents the verification statistics for the average daily T2 and DSW among all sites. As shown in Table 2, the mean error (ME), mean bias (MB), correlation coefficient (r) and root mean square error (RMSE) of station-averaged hourly T2 series are 2.47, −1.26, 0.95 and 2.59 °C, respectively. The simulation yields cooling biases of −0.98, −0.90, −1.70 and −1.18 °C in spring, summer, fall and winter, respectively. The ME, MB, r and RMSE values for the annual DSW series are 36.00, -29.88, 0.80 and 81.33 W m^{-2}, and the DSW simulation yields underestimations of 32.12, 43.61, 24.25 and 19.38 W m^{-2} in spring, summer, fall and winter, respectively. It is because that the WRF model overestimate the cloud coverage which lead to the slightly underestimation on T2 and DSW (Wang et al., 2010; Wen et al., 2014). Compared with other studies on yearly long WRF simulation in China (Wang et al., 2014; Ying et al., 2014; Zhang et al., 2012), these biases are relatively small and the simulations on temperature and radiation are correlated with the observations under a confidence level of 0.01, indicating both seasonally and yearly significant correlations in this study. Therefore, the WRF model performances of meteorological conditions can be considered reasonable for driving MEGAN.

179 **Table 2.** Verification statistics for the WRF simulations of temperature at 2 m (T2) and
180 downward shortwave radiation (DSW).

Variable	Season	Mean		ME	MB	*r*	RMSE
		Obs.	Sim.				
T2 (°C)	Spring	14.47	13.49	2.03	-0.98	0.96	2.26
	Summer	25.31	24.41	1.72	-0.90	0.95	2.21
	Fall	14.49	12.79	2.43	-1.70	0.92	2.45
	Winter	3.04	1.86	2.67	-1.18	0.94	3.28
	Year	14.32	13.06	2.47	-1.26	0.95	2.59
DSW (W m^{-2})	Spring	200.80	232.92	37.09	-32.12	0.83	72.36
	Summer	229.85	273.46	52.33	-43.61	0.75	84.15
	Fall	137.93	162.18	30.85	-24.25	0.86	60.52
	Winter	108.30	127.68	23.72	-19.38	0.92	42.28
	Year	169.18	199.06	36.00	-29.88	0.84	62.83

181 ME: mean error; MB: mean bias; RMSE: root mean square error.

182 Table 3 illustrates the estimated annual emissions of BVOCs in this work and other
183 studies. The estimate of annual BVOC emissions was 23.54 Tg, which is within the range
184 reported in previous estimates, ranging from 12.83 Tg to 42.5 Tg between 1990 and 2006.
185 Estimates in the present work are greater than the 20.6 Tg for 2000 estimated by Klinger et al.
186 (2002) and 12.83 Tg for 2003 estimated by Chi et al. (2011). However, the estimates in the
187 present study are lower than the results of Guenther et al. (1995) and Li et al. (2013), who
188 obtained values of 28.4 Tg for 1990 and 42.5 Tg for 2003, respectively. Differences among the
189 discussed studies can be attributed to various factors. It is reported that the forest coverage, the
190 percentage of which increased from 16.6% in 2003 to 21.63% in 2014, and the forest area
191 increased from 1.59×10^8 hm^2 in 2003 to 2.08×10^8 hm^2 in 2014 (CFB, 2014), which may be the
192 main reasons for large discrepancies. In addition, BVOC emissions were largely followed by
193 LAI changes (Souri et al., 2017). Chen et al. (2019) utilized satellite data to analyze the annual

194 average MODIS LAI in China from 2000-2017 and observed a significant increasing trend in
195 eastern China (the trend was higher than 18×10^{-2} m^2 per m^2 per decade; see Fig. S3 in the
196 Supporting Information). Therefore, the interannual variation of LAI is also an important factor
197 which cause the differences. Besides, some of the discrepancies can also be explained by the use
198 of different algorithms and emission factors. In this study, the MEGAN default global average
199 EFs were applied to estimate BVOC emissions. Li et al. (2012) used a simplified isoprene
200 algorithm (PCEEA) and neglected the effect of soil moisture and detailed canopy information,
201 which resulted in a much lower estimate of 12.97 Tg in 2006 than our study. Fu and Liao (2012)
202 adopted lower EFs and leaf biomass densities for each plant type derived from a small number of
203 local measurements, which caused an underestimation of emissions. There is a large difference
204 of isoprene emission between our results and those of Klinger et al. (2002). It is mainly because
205 that Klinger et al. (2002) did not include emissions from the shrubs and assumed that BVOC
206 emissions emitted from forests in China with 251,283 km^2 which is smaller than the domain of
207 our study. Therefore, variations in these factors in different years may be the cause of the
208 uncertainty in the modeling simulations. However, large discrepancies in the emission estimates
209 still exist among this study and previous studies. These differences result from the use of
210 different emission factors, land cover distributions, meteorological conditions and model
211 algorithms in developing the emission inventories, as discussed above.

212 **Table 3.** Comparison of previous BVOC emission estimations in China (unit: Tg yr^{-1}).

Method	Area	ISOP	TERP	OVOCs	Total BVOCs	Year(s)	Reference
MEGAN	China	13.3	3.09	7.15	23.54	2017	This study
MEGAN	China	15	4.3	9.1	28.4	1990	Guenther et al. (1995)
MEGAN	China	4.1	3.5	13	20.6	2000	Klinger et al. (2002)
MEGAN	China	7.45	2.23	3.14	12.83	2003	Chi and Xie (2011)
MEGAN	China	20.7	4.9	13.5	42.5	2003	Li et al. (2013)

MEGAN	China	7.7	3.16	\	\	2004	Tie et al. (2006)
MEGAN	China	9.36	3.61	\	12.97	2006	Li et al. (2012)
MEGAN	China	9.59	2.83	\	\	2001-2006	Fu et al. (2012)

OVOCs: other VOCs

3.2 Spatial distribution of BVOC emissions

BVOC emissions exhibit overt spatial variations due to the differences in vegetation types, topography and climatic conditions. Previous studies have shown that broadleaf forests and shrubs have strong isoprene emission potentials, coniferous forests have high terpene emission potential, and crops and grasses are generally considered to have low or no isoprene emissions (Wiedinmyer et al., 2006; Chen et al., 2018). Therefore, the distribution of high isoprene emissions is generally associated with the distribution of broadleaf forests and shrubs.

As shown in Fig. 4, BVOC emissions in China are mostly centralized in the northeast and southeast and in southern Yunnan, Hainan and Taiwan Provinces. Specifically, the forest area in Yunnan accounts for nearly 10% of all forest cover in China. Therefore, Yunnan Province has the highest BVOC emissions, and the large area of tropical rainforest cover in southern Yunnan leads to substantially higher BVOC emissions in the southern region than in other regions. The high emissions in the northeast are due to the high forest coverage of the genus and eucalyptus forest which have the highest isoprene emission potential. Taiwan's high emissions originate from evergreen broadleaf forests. The distribution of various deciduous, hardwood and mixed broadleaf trees account for the high emissions in southeastern China and the Qinglin Mountains. Owing to the wide coverage of tropical rainforests, the BVOC emissions in Hainan Province are consequently high. Because of the principal contribution of isoprene to total BVOCs, the spatial distribution of total BVOC emissions is similar to that of forest distribution. Terpene emissions are concentrated in the southern part of China (especially in the southeast) because of the high-

density coniferous forests there. In southwestern China, especially in the Sichuan-Tibet region, high altitudes and low temperatures on the Tibetan Plateau have led to low levels of emissions in the region. In the Sichuan Basin (SCB), although the forest and shrub coverages are high, isoprene emissions are relatively low. This trend may be caused by the low temperatures in western Sichuan and the low solar radiation in eastern Sichuan, coupled with the closed terrain and extensive cloud cover in the atmosphere (Lin et al., 2016). In addition, high OVOC emissions lead to high total BVOC emissions in most parts of southern China.

3.3 Seasonal variations

The modeling results from this study indicate different seasonal BVOC emissions in China (Fig. 5). Isoprene and terpene are the most dominant BVOC emissions. The quantity of seasonal BVOC emissions varies as follows: summer > spring > autumn > winter. The distribution pattern of isoprene in spring and autumn is quite consistent and mainly concentrated in southern China due to the relatively dense vegetation cover in southern China. Additionally, decreasing temperature and solar radiation from south to north contribute to the distribution of isoprene emissions in southern China. In summer, eastern China has high temperatures, intense radiation and vigorous forest growth, subsequently resulting in obviously higher BVOC emissions. Except for Inner Mongolia, which is dominated by grassland desert, the monthly emission intensities of isoprene and terpene are 30×10^6 g/month or higher in most areas. Due to dieback of vegetation and the presence of snow cover in winter, which cause the LAI to sharply decrease, the emissions of isoprene and terpene are relatively low (generally below 4×10^6 g/month), especially in the northeastern region, where temperate deciduous forests are dominant.

Fig. 6 illustrates the different monthly evolution patterns of BVOC emissions in China. BVOC emissions are concentrated between April and September and reach a maximum of 5.8

Tg in June. As seasons transit, accompanied by a decrease in temperature, radiation and vegetation cover, the emissions intensity of BVOC drops sharply and reaches a minimum of 23 Tg in December. The monthly isoprene emissions oscillated between the maximum (3.56 Tg) in July and the minimum (0.09 Tg) in December. The monthly emissions of monoterpene are similar to those of isoprene, which reach a peak of 0.64 Tg in July and a bottom of 0.05 Tg in December. It is noteworthy that the relative contribution of isoprene to monthly total BVOC emissions ascends from January to July and descends from July to December, while terpene and sesquiterpene do not exhibit this characteristic and their seasonal changes are not as obvious as that of isoprene. Therefore, we can reach a conclusion that isoprene is more sensitive than terpene and sesquiterpene to seasonal changes.

3.4 Impact of BVOC emissions on summertime O_3 and SOA formation in 2017

Since the control of precursors can only be directed at anthropogenic rather than biogenic emissions, it is of great importance to understand how biogenic emissions interact with anthropogenic emissions and contribute to air quality that is below national standards. Therefore, to further investigate the influence of BVOC emissions on SOA and ozone in China, we performed three parallel CMAQ simulations, the first of which included both anthropogenic and biogenic emissions, while the NB case only considered anthropogenic emissions to quantify the effects of BVOC emissions on ground-level ozone in the real atmosphere, and the NA case excluded anthropogenic emissions to reflect a clean atmosphere (see Fig. S5 in supporting information).

Fig.7a–c shows the simulated and observed daily 1-h maximum O_3 ($DM1O_3$) concentration over China in July 2017. In general, the model successfully captured the spatial pattern over the simulated domain with highest $DM1O_3$ areas centralized in the east, especially

in the BTH, PRD, YRD and SCB regions due to the relatively large NO_x and VOC emission and favorable meteorological conditions for ozone formation in these areas (e.g., little rain and strong solar radiation). And model performance of $DM1O_3$ in different regions is evaluated in Table 4. As shown in Table 4 and Fig.7, the model well reproduced $DM1O_3$ in most cities except for slightly underestimates $DM1O_3$ concentrations in BTH, YRD, PRD and SCB. The underestimation might be caused by uncertainty of meteorological condition simulated by WRF (such as T2 and DSW discussed in section 3.1). Besides, the relatively coarse spatial resolution in the model and underestimation of anthropogenic emissions in these megacities may also contribute to the underestimation.

As shown in Fig.7d-e, ozone concentration simulated by NB case is significantly higher than NA case which indicated that effect of biogenic emissions on ozone concentration is less than that of anthropogenic emissions. To clarify the change in ozone concentration after removal of BVOC, Fig. 8 shows the relative difference in ozone concentration with/without BVOC emissions. The high BVOC emissions across the eastern and southwestern areas of China increased $DM1O_3$, particularly in BTH, YRD, SCB and central PRD, by up to 47 μg m^{-3}. This phenomenon is likely due to the combined effects of BVOC emissions and O_3-NOx-VOC sensitivity in these regions. As shown in Fig. 5, the major source of BVOCs in July is isoprene and terpene, which are most abundant in summer (discussed in Section 3.3). In addition, Jin and Holloway (2015) reported that the NOx-limited regime is dominant in southern China and that northern China is dominated by VOC-limited and transitional regimes (see Fig. S4 in the Supporting Information). In areas (especially rural areas) where NOx is limited but VOC emissions are already abundant, biogenic emissions have little effect on ozone formation; in

areas where VOC emissions are low, however, mounting VOC emissions (i.e., inclusion of biogenic emissions) will result in more ozone formation.

Fig. 9 presents the SOA concentrations simulated by base case, NA and NB case, respectively. In summer, SOA concentrations in central and eastern China typically exceed 1 μg m^{-3} and can reach up to 3 μg m^{-3}. There is also a relatively high SOA concentration in other southern provinces and the Sichuan Basin. The simulated SOA concentrations are low in northern and northeastern China. Removing anthropogenic VOC emissions in July causes a decrease of SOA in major areas by relative change of approximately 60% while eliminating biogenic emissions results in an approximately 70% reduction of the simulated SOA concentrations. Therefore, the removal of biogenic emissions affects both biogenic and anthropogenic compounds of SOA.

As shown in Fig. 10, biogenic emissions are the most important contributors to SOA in summer. In China, biogenic emissions account for approximately 70% of SOA. In most areas, biogenic emissions are the most crucial contributors; even in areas where there are no significant isoprene emissions, the relative contribution of biogenic emissions to SOA formation is as high as 80% (Hu et al., 2017; Wang et al., 2018). In addition, due to the influence of the summer monsoon, precursors from high biogenic emissions in southern China are transported to central and northern China. High temperatures and intense solar radiation in summer enhance biogenic VOC emissions and photochemical generation of SOA, resulting in high national contributions of biogenic emissions to the formation of SOA. Xu et al. (2015) showed that monoterpene-derived SOA are mediated by SO_2 and NOx. By providing an absorptive organic mass, the biogenic compounds of particles facilitate the condensation of anthropogenic compounds. The SOA yield of the oxidized products of monoterpene and isoprene can be enhanced at high NOx

concentrations, favoring the formation of organic nitrate, which is a low-volatility product and is likely to partition into seed particles. When the NOx level is low, isoprene oxidation occurs via the ISOPOOH pathway to form IEPOX-SOA, which favorably forms organic sulfate in acidic environments. This reaction has been incorporated into CMAQ; thus, the inclusion of both anthropogenic and biogenic emissions reflects these products, but including only one of them is unable to account for their reaction.

Table 4. Model performance on $DM1O_3$ in different regions during July 2017 (Units: μg m^{-3})

		BTH	YRD	PRD	SCB	Other	China
O_3-1h	Obs.	198.2	170.5	110.4	185.6	137.6	160.5
	Sim.	173.1	156.3	102.3	173.4	124.6	145.9
	MB	-25.1	-14.2	-8.1	-12.2	-13.0	-14.6
	ME	27.3	16.2	10.2	14.4	16.7	18.1
	r	0.82	0.85	0.92	0.90	0.87	0.86

3.5 Discussion of uncertainties in model driving variables

The meteorological parameters, emission factors and parameterization method are essential driving variables for MEGAN and the uncertainties of estimated BVOC emissions and their corresponding impacts on surface ozone and SOA are related with uncertainties in these inputs (Hogrefe et al., 2011; Jiang et al., 2019). In this part, we discussed the uncertainties to better understand the results and improve future research directions.

3.5.1 Meteorological parameters

The WRF model performance in this study was comparable to other studies (Wang et al., 2014; Hu et al., 2016; Zhang et al., 2012). Although we employed four-dimensional data assimilation for improving model performance, some meteorological parameters are still biased. For example, the WRF model underestimated T2 and DSW, especially in summer. On the one hand, considering the significant impact of solar radiation and temperature on photochemical

reaction, underestimation of T2 and DSW may lead to corresponding underestimation on BVOC emission and ozone. On the other hand, it may cause underestimation on SOA because it is expected to form more SOA due to higher VOCs emissions and higher atmospheric reactivity during summer. Therefore, improvements on WRF model capability are urgently needed for accurate BVOC estimation.

3.5.2 Parameterization method

It has been reported that soil moisture could impact biogenic emissions and subsequent ozone concentrations (Wang et al., 2017; Jiang et al., 2018). In our study, soil moisture is simulated by using Noah Land Surface Model parameterization in WRF. And the reduction of isoprene emissions due to potential soil moisture limitation was not considered because MEGAN 2.1 simplified soil moisture's impact on BVOC estimation. Hence, soil moisture's impact on BVOC estimation should be considered by further detailed parameterization method in future research.

4 Conclusion

In this study, we utilized MEGAN to estimate the BVOC emissions in 2017 throughout China, then further applied the WRF-CMAQ model to quantify the contributions of BVOCs to surface ozone and SOA formation in China in July 2017. BVOC emissions in China were estimated to be 23.54 Tg in 2017, decreasing from south to north, which is related to the vegetation distribution. Additionally, BVOC emissions exhibited strong seasonal variations due to changes in temperature and solar radiation, with the highest emissions in summer.

Ozone concentrations mainly peaked in the eastern and southwestern China, particularly in the BTH, YRD, PRD and SCB regions because of their considerably large NOx and VOC emission sources and advantageous meteorological conditions for ozone formation. Even though

368 the effect of biogenic emissions on O_3 is less profound than that of anthropogenic emissions (as
369 shown in Fig.7(d)(e)), the BVOC emissions still made a significant contribution to summertime
370 ozone due to the influence of the southerly wind, transporting precursors from high biogenic
371 emission regions in southern China to central China and the BTH area. And the regions where
372 the influence of biogenic emissions is high match with those where ozone formation is VOC
373 limited.

374 BVOC emissions make a large contribution to summertime SOA (national average of
375 70%). Locally, the effects of biogenic emissions tend to be greater in the southern region than in
376 the northern region, as the megacities are surrounded by regions of high biogenic emissions. In
377 summer, the impact of biogenic emissions on SOA is much greater than that of anthropogenic
378 emissions. However, the impact of anthropogenic emissions in individual regions may be rather
379 high (up to 50%), indicating that even BSOA can be significantly controlled by limiting
380 anthropogenic emissions. When anthropogenic emissions are not considered, the reduction in
381 BSOA depends on the chemical precursor. In particular, isoprene SOA is more easily reduced
382 than monoterpene SOA due to their different volatilities. ASOA are also affected by biogenic
383 emissions (the absorption of organic matter by SOA), and the relative impact may be as high as
384 40%. In order to accurately simulate SOA, it is necessary to precisely simulate both ASOA and
385 BSOA (Pye et al., 2019).

386 It should be noted that the simulated SOA concentrations in this study have not been
387 compared with direct measurements of organic particulate matter and SOA because of the data
388 limitations. Extensive measurements of organic components have been conducted in megacities
389 and major clusters in China by aerosol mass spectrometers (AMS), which provides details about
390 various organic aerosols (Hu et al., 2016; Yang et al., 2016). And these data can be used as

model validation for future local scale SOA modeling studies which can promote the understanding of SOA formation. Besides, a great deal of additional research is needed to further address the remaining questions. For example, to better quantify the separate and synergistic effects of anthropogenic and VOC emissions based on sensitivity testing, it is necessary to investigate the spatial distribution of ozone changes by comparing NOx and VOC emissions. Both chamber studies and field measurements have shown that HOMs (highly oxygenated molecules) can substantially increase the SOA mass because of their low volatility (Ehn et al., 2014). This mechanism has already been incorporated into box models (Öström et al., 2017) with detailed chemistry, and it would be interesting to observe the impact of this mechanism on SOA formation from BVOCs at the regional scale.

Author contributions

The manuscript was written through contributions of all authors. All authors have given approval to the final version of the manuscript

Acknowledgements

This work was funded by the the National Key Research and Development Program of China (No.2018YFC0214002), the Basic Applied Research Project of Science and Technology Plan of Sichuan Province (No.2018JY0011), the Key Project of Science and Technology Plan of Sichuan Province (No.2018SZDZX0023) and the Scientific Research Foundation of Chengdu University of Information Technology (No.KYTZ201731 and KYTZ201814). The meteorological dataset was provided by the China Meteorological Data Sharing Service System (http://cdc.cma.gov.cn). Additionally, the air pollutant data were downloaded from the National Urban Air Quality Real-time Publishing Platform (http://106.37.208.233:20035/). The datasets

generated during and/or analyzed in this study are publicly available as referenced within the article. All data and scripts are available from the corresponding author upon request.

References

Arneth, A., Schurgers, G., Lathiere, J., Duhl, T., Beerling, D.J., Hewitt, C.N., Martin, M., Guenther, A., 2011. Global terrestrial isoprene emission models: sensitivity to variability in climate and vegetation. Atmos. Chem. Phys. 11, 8037–8052. doi:10.5194/acp-11-8037-2011.

China Forestry Bureau (CFB), 2014. China Forestry Database. http://www.forestry.gov.cn/data.html (last accessed on 7.18.2019).

Chen, C., Park, T., Wang, X., Piao, S., Xu, B., Chaturvedi, R.K., Fuchs, R., Brovkin, V., Ciais, P., Fensholt, R., Tømmervik, H., Bala, G., Zhu, Z., Nemani, R.R., Myneni, R.B., 2019. China and India lead in greening of the world through land-use management. Nat. Sustain. 2, 122–129. doi:10.1038/s41893-019-0220-7.

Chen, W.H., Guenther, A.B., Wang, X.M., Chen, Y.H., Gu, D.S., Chang, M., Zhou, S.Z., Wu, L.L., Zhang, Y.Q., 2018. Regional to global biogenic isoprene emission responses to changes in vegetation from 2000 to 2015. J. Geophys. Res. Atmos. 123, 3757–3771. doi:10.1002/2017jd027934.

Chi, Y.Q., Xie, S.D., 2011. Spatiotemporal inventory of biogenic volatile organic compound emissions in China based on vegetation volume and production. In: International Conference on Energy, Environment and Sustainable Development (ICEESD 2011). Shanghai Univ Elect Power, Shanghai, Peoples R China,pp. 2579e2582

Ding, X., He, Q.-F., Shen, R.-Q., Yu, Q.-Q., Wang, X.-M., 2014. Spatial distributions of secondary organic aerosols from isoprene, monoterpenes, β-caryophyllene, and aromatics

436 over China during summer. J. Geophys. Res. Atmos. 119, 11, 877–811, 891.
437 doi:10.1002/2014JD021748.
438 Ehn, M., Thornton, J.A., Kleist, E., Sipilä, M., Junninen, H., Pullinen, I., Springer, M., Rubach,
439 F., Tillmann, R., Lee, B., Lopez-Hilfiker, F., Andres, S., Acir, I.-H., Rissanen, M.,
440 Jokinen, T., Schobesberger, S., Kangasluoma, J., Kontkanen, J., Nieminen, T., Kurtén, T.,
441 Nielsen, L.B., Jørgensen, S., Kjaergaard, H.G., Canagaratna, M., Maso, M.D., Berndt, T.,
442 Petäjä, T., Wahner, A., Kerminen, V.-M., Kulmala, M., Worsnop, D.R., Wildt, J., Mentel,
443 T.F., 2014. A large source of low-volatility secondary organic aerosol. Nature 506, 476.
444 doi:10.1038/nature13032.
445 Foroutan, H., Young, J., Napelenok, S., Ran, L., Appel, K.W., Gilliam, R.C., & Pleim, J.E., 2017.
446 Development and evaluation of a physics-based windblown dust emission scheme
447 implemented in the CMAQ modeling system, J. Advances in Modeling Earth Systems 7,
448 1–26. doi:10.1002/2016MS000823
449 Graedel, T., Bates, T., Bouwman, A., Cunnold, D., Dignon, J., Fung, I., J. Jacob, D., Lamb, B.,
450 Logan, J., Marland, G., Middleton, P., M. Pacyna, J., 1993. A compilation of inventories
451 of emissions to the atmosphere. Glob. Biogeochem. Cycles 7, 1–26.
452 doi:10.1029/92GB02793.
453 Gu, D., Guenther, A.B., Shilling, J.E., Yu, H., Huang, M., Zhao, C., Yang, Q., Martin, S.T.,
454 Artaxo, P., Kim, S., Seco, R., Stavrakou, T., Longo, K.M., Tóta, J., de Souza, R.A.F.,
455 Vega, O., Liu, Y., Shrivastava, M., Alves, E.G., Santos, F.C., Leng, G., Hu, Z., 2017.
456 Airborne observations reveal elevational gradient in tropical forest isoprene emissions.
457 Nat. Commun. 8, 15541. doi:10.1038/ncomms15541.

458 Guenther, A.B., Jiang, X., Heald, C.L., Sakulyanontvittaya, T., Duhl, T., Emmons, L.K.,
459 Wang, X., 2012. The model of emissions of gases and aerosols from nature version 2.1
460 (MEGAN2.1): an extended and updated framework for modeling biogenic emissions.
461 Geosci. Model Dev. 5, 1471–1492. doi:10.5194/gmd-5-1471-2012.
462 Guenther, A., Hewitt, C.N., Erickson, D., Fall, R., Geron, C., Graedel, T., Harley, P.,
463 Klinger, L., Lerdau, M., Mckay, W.A., Pierce, T., Scholes, B., Steinbrecher, R.,
464 Tallamraju, R., Taylor, J., Zimmerman, P., 1995. A global model of natural volatile
465 organic compound emissions. J. Geophys. Res. Atmos. 100, 8873–8892.
466 doi:10.1029/94jd02950.
467 Guenther, A., Karl, T., Harley, P., Wiedinmyer, C., Palmer, P.I., Geron, C., 2006.
468 Estimates of global terrestrial isoprene emissions using MEGAN (Model of emissions of
469 gases and aerosols from nature). Atmos. Chem. Phys. 6, 3181–3210. doi:10.5194/acp-6-
470 3181-2006.
471 Hallquist, M., Wenger, J.C., Baltensperger, U., Rudich, Y., Simpson, D., Claeys, M., Dommen,
472 J., Donahue, N.M., George, C., Goldstein, A.H., Hamilton, J.F., Herrmann, H., Hoffmann,
473 T., Iinuma, Y., Jang, M., Jenkin, M.E., Jimenez, J.L., Kiendler-Scharr, A., Maenhaut, W.,
474 McFiggans, G., Mentel, T.F., Monod, A., Prévôt, A.S.H., Seinfeld, J.H., Surratt, J.D.,
475 Szmigielski, R., Wildt, J., 2009. The formation, properties and impact of secondary
476 organic aerosol: current and emerging issues. Atmos. Chem. Phys. 9, 5155–5236.
477 doi:10.5194/acp-9-5155-2009.
478 Hantson, S., Knorr, W., Schurgers, G., Pugh, T.A.M., Arneth, A., 2017. Global isoprene and
479 monoterpene emissions under changing climate, vegetation, CO2 and land use. Atmos.
480 Environ. 155, 35–45. doi:10.1016/j.atmosenv.2017.02.010.

481 Jiang, X., Guenther, A., Potosnak, M., Geron, C., Seco, R., Karl, T., Kim, S., Gu, L., Pallardy, S.,
482 2018. Isoprene emission response to drought and the impact on global atmospheric
483 chemistry. Atmos. Environ. 183, 69–83. doi:10.1016/j.atmosenv.2018.01.026.
484 Jin, X., Holloway, T., 2015. Spatial and temporal variability of ozone sensitivity over China
485 observed from the ozone monitoring instrument. J. Geophys. Res. Atmos. 120, 7229–
486 7246. doi:10.1002/2015jd023250.
487 Klinger, L.F., Li, Q.-J., Guenther, A.B., Greenberg, J.P., Baker, B., Bai, J.-H., 2002. Assessment
488 of volatile organic compound emissions from ecosystems of China. J. Geophys. Res.
489 Atmos. 107, ACH 16–11–ACH 16–21. doi:10.1029/2001jd001076.
490 Kulmala, M., Suni, T., Lehtinen, K.E.J., Dal Maso, M., Boy, M., Reissell, A., Rannik, Ü., Aalto,
491 P., Keronen, P., Hakola, H., Bäck, J., Hoffmann, T., Vesala, T., Hari, P., 2004. A new
492 feedback mechanism linking forests, aerosols, and climate. Atmos. Chem. Phys. 4, 557–
493 562. doi:10.5194/acp-4-557-2004.
494 Li, L.Y., Chen, Y., Xie, S.D., 2013. Spatio-temporal variation of biogenic volatile organic
495 compounds emissions in China. Environ. Pollut. 182, 157–168.
496 doi:10.1016/j.envpol.2013.06.042.
497 Li, L.Y., Xie, S.D., 2014. Historical variations of biogenic volatile organic compound emission
498 inventories in China, 1981–2003. Atmos. Environ. 95, 185–196.
499 doi:10.1016/j.atmosenv.2014.06.033.
500 Li, M., Huang, X., Li, J., Song, Y., 2012. Estimation of biogenic volatile organic compound
501 (BVOC) emissions from the terrestrial ecosystem in China using real-time remote
502 sensing data. Atmos. Chem. Phys. Discuss.12, 6551–6592. doi:10.5194/acpd-12-6551-
503 2012.

Makkonen, R., Asmi, A., Kerminen, V.M., Boy, M., Arneth, A., Guenther, A., Kulmala, M., 2012. BVOC-aerosol-climate interactions in the global aerosol-climate model ECHAM5.5-HAM2. Atmos. Chem. Phys. 12, 10077–10096. doi:10.5194/acp-12-10077-2012.

Mo, Z., Shao, M., Wang, W., Liu, Y., Wang, M., Lu, S., 2018. Evaluation of biogenic isoprene emissions and their contribution to ozone formation by ground-based measurements in Beijing, China. Sci. Total Environ. 627, 1485–1494. doi:10.1016/j.scitotenv.2018.01.336.

Öström, E., Putian, Z., Schurgers, G., Mishurov, M., Kivekäs, N., Lihavainen, H., Ehn, M., Rissanen, M.P., Kurtén, T., Boy, M., Swietlicki, E., Roldin, P., 2017. Modeling the role of highly oxidized multifunctional organic molecules for the growth of new particles over the boreal forest region. Atmos. Chem. Phys. 17, 8887–8901. doi:10.5194/acp-17-8887-2017.

Ou, J., Zheng, J., Li, R., Huang, X., Zhong, Z., Zhong, L., Lin, H., 2015. Speciated OVOC and VOC emission inventories and their implications for reactivity-based ozone control strategy in the Pearl River Delta region, China. Sci. Total Environ. 530-531, 393–402. doi:10.1016/j.scitotenv.2015.05.062.

Paasonen, P., Asmi, A., Petäjä, T., Kajos, M.K., Äijälä, M., Junninen, H., Holst, T., Abbatt, J.P.D., Arneth, A., Birmili, W., van der Gon, H.D., Hamed, A., Hoffer, A., Laakso, L., Laaksonen, A., Leaitch, W., Plass-Dülmer, C., Pryor, S.C., Räisänen, P., Swietlicki, E., Wiedensohler, A., Worsnop, D.R., Kerminen, V.-M., Kulmala, M., 2013. Warming-induced increase in aerosol number concentration likely to moderate climate change. Nat. Geosci. 6, 438. doi:10.1038/ngeo1800

526 Pan, X., Kanaya, Y., Tanimoto, H., Inomata, S., Wang, Z., Kudo, S., Uno, I., 2015. Examining
527 the major contributors of ozone pollution in a rural area of the Yangtze River Delta
528 region during harvest season. Atmos. Chem. Phys. 15, 6101–6111. doi:10.5194/acp-15-
529 6101-2015.
530 Pye, H.O.T., D'Ambro, E.L., Lee, B.H., Schobesberger, S., Takeuchi, M., Zhao, Y., Lopez-
531 Hilfiker, F., Liu, J., Shilling, J.E., Xing, J., Mathur, R., Middlebrook, A.M., Liao, J.,
532 Welti, A., Graus, M., Warneke, C., de Gouw, J.A., Holloway, J.S., Ryerson, T.B., Pollack,
533 I.B., Thornton, J.A., 2019. Anthropogenic enhancements to production of highly
534 oxygenated molecules from autoxidation. Proc. Natl. Acad. Sci. U. S. A. 116, 6641–6646.
535 doi:10.1073/pnas.1810774116.
536 Qin, M., Wang, X., Hu, Y., Ding, X., Song, Y., Li, M., Vasilakos, P., Nenes, A., Russell, A.G.,
537 2018. Simulating biogenic secondary organic aerosol during summertime in China. J.
538 Geophys. Res. Atmos. 123, 11100–111119. doi:10.1029/2018jd029185.
539 Situ, S., Guenther, A., Wang, X., Jiang, X., Turnipseed, A., Wu, Z., Bai, J., Wang, X., 2013.
540 Impacts of seasonal and regional variability in biogenic VOC emissions on surface ozone
541 in the Pearl River Delta region, China. Atmos. Chem. Phys. 13, 11803–11817.
542 doi:10.5194/acp-13-11803-2013
543 Tie, X.X., Li, G.H., Ying, Z.M., Guenther, A., Madronich, S., 2006. Biogenic emissions of
544 isoprenoids and NO in China and comparison to anthropogenic emissions. Sci of the
545 Total Environ 371, 238-251 doi:10.1016/j.scitotenv.2006.06.025
546 Tsui, J.K.-Y., Guenther, A., Yip, W.-K., Chen, F., 2009. A biogenic volatile organic compound
547 emission inventory for Hong Kong. Atmos. Environ. 43, 6442–6448.
548 doi:10.1016/j.atmosenv.2008.01.027.

549 Wiedinmyer, C., Tie, X., Guenther, A., Neilson, R., Granier, C., 2006. Future changes in
550 biogenic isoprene emissions: how might they affect regional and global atmospheric
551 chemistry? Earth Interact. 10, 1–19. doi:10.1175/EI174.1.
552 Xu, L., Guo, H., Boyd, C.M., Klein, M., Bougiatioti, A., Cerully, K.M., Hite, J.R., Isaacman-
553 VanWertz, G., Kreisberg, N.M., Knote, C., Olson, K., Koss, A., Goldstein, A.H., Hering,
554 S.V., de Gouw, J., Baumann, K., Lee, S.-H., Nenes, A., Weber, R.J., Ng, N.L., 2015.
555 Effects of anthropogenic emissions on aerosol formation from isoprene and
556 monoterpenes in the southeastern United States. Proc. Natl. Acad. Sci. U. S. A. 112, 37–
557 42. doi:10.1073/pnas.1417709112.
558 Yu, F., Hong, L., 2012. Simulation of the interannual variations of biogenic emissions of volatile
559 organic compounds in China: Impacts on tropospheric ozone and secondary organic
560 aerosol. Atmos. Environ. 59, 170–185. doi:10.1016/j.atmosenv.2012.05.053.
561 Hu, J., Wang, P., Ying, Q., Zhang, H., Chen, J., Ge, X.,. 2017. Modeling biogenic and
562 anthropogenic secondary organic aerosol in China. Atmos. Chem. Phys., 17(1), 77-92.
563 Hogrefe, C., Pouliot, G., Wong, D., Torian, A., Roselle, S., Pleim, J. and Mathur, R. 2015.
564 Annual application and evaluation of the online coupled WRF–CMAQ system over
565 North America under AQMEII phase 2. Atmos. Environ, 115, 683-694.
566 Xing, J., Mathur, R., Pleim, J., Hogrefe, C., Gan, C.M., Wong, D.C. and Wei, C. 2015. Can a
567 coupled meteorology–chemistry model reproduce the historical trend in aerosol direct
568 radiative effects over the Northern Hemisphere ?. Atmos. Chem. Phys. 15(17), 9997-
569 10018.

570 Xing, J., Wang, J., Mathur, R., Wang, S., Sarwar, G., Pleim, J., 2017. Impacts of aerosol direct
571 effects on tropospheric ozone through changes in atmospheric dynamics and photolysis
572 rates. Atmos. Chem. Phys., 17(16), 9869-9883.
573 Appel, K. W., Pouliot, G. A., Simon, H., Sarwar, G., Pye, H. O. T., Napelenok, S. L., et al.
574 (2013). Evaluation of dust and trace metal estimates from the Community Multiscale Air
575 Quality (CMAQ) model version 5.0. Geosci. Model Dev., 6(4), 883-899.
576 https://www.geosci-model-dev.net/6/883/2013/
577 Carlton, A. G., Bhave, P. V., Napelenok, S. L., Edney, E. O., Sarwar, G., Pinder, R. W., et al.
578 (2010). Model Representation of Secondary Organic Aerosol in CMAQv4.7.
579 Environmental Science & Technology, 44(22), 8553-8560. doi:10.1021/es100636q
580 Murphy, B. N., Woody, M. C., Jimenez, J. L., Carlton, A. M. G., Hayes, P. L., Liu, S., et al.
581 (2017). Semivolatile POA and parameterized total combustion SOA in CMAQv5.2:
582 impacts on source strength and partitioning. Atmos. Chem. Phys., 17(18), 11107-11133.
583 https://www.atmos-chem-phys.net/17/11107/2017/
584 Pye, H. O. T., Murphy, B. N., Xu, L., Ng, N. L., Carlton, A. G., Guo, H., et al. (2017). On the
585 implications of aerosol liquid water and phase separation for organic aerosol mass.
586 Atmos. Chem. Phys., 17(1), 343-369. https://www.atmos-chem-phys.net/17/343/2017/
587 Simon, H., & Bhave, P. V. (2012). Simulating the Degree of Oxidation in Atmospheric Organic
588 Particles. Environmental Science & Technology, 46(1), 331-339. doi:10.1021/es202361w
589 Souri, A. H., Choi, Y., Jeon, W., Woo, J.-H., Zhang, Q., & Kurokawa, J.-i. (2017). Remote
590 sensing evidence of decadal changes in major tropospheric ozone precursors over East
591 Asia. Journal of Geophysical Research: Atmospheres, 122(4), 2474-2492.
592 doi:10.1002/2016JD025663

Hu, W., Hu, M., Hu, W., Jimenez, J. L., Yuan, B., Chen, W., Wang, M., Wu, Y., Chen, C., Wang, Z., Peng, J., Zeng, L., and Shao, M.: Chemical composition, sources, and aging process of submicron aerosols in Beijing: Contrast between summer and winter, Journal of Geophysical Research: Atmospheres, 121, 1955-1977

Yang, F., Kawamura, K., Chen, J., Ho, K., Lee, S., Gao, Y., Cui, L., Wang, T., and Fu, P.: Anthropogenic and biogenic organic compounds in summertime fine aerosols (PM2.5) in Beijing, China, Atmospheric Environment, 124, Part B, 166-175, doi:10.1016/j.atmosenv.2015.08.095, 2016.

Wang, Y., Xie, Y., Dong, W., Ming, Y., Wang, J., & Shen, L. (2017). Adverse effects of increasing drought on air quality via natural processes. Atmos. Chem. Phys., 17(20), 12827-12843.

Jiang, X., Guenther, A., Potosnak, M., Geron, C., Seco, R., Karl, T., et al. (2018). Isoprene emission response to drought and the impact on global atmospheric chemistry. Atmospheric Environment, 183, 69-83.

Wen, X., Liao, X., Yuan, W., Yan, X., Wei, Z., Liu, H., et al. (2014). Numerical simulation and data assimilation of the water-energy cycle over semiarid northeastern China. Science China Earth Sciences, 57(10), 2340-2356. doi:10.1007/s11430-014-4914-4

Ying, Q., Wu, L., and Zhang, H.: Local and inter-regional contributions to PM2:5 nitrate and sulfate in China, Atmos. Environ., 94, 582–592, 2014b.

Zhang, H., Li, J., Ying, Q., Yu, J. Z., Wu, D., Cheng, Y., He, K., and Jiang, J.: Source apportionment of PM2:5 nitrate and sulfate in China using a source-oriented chemical transport model, Atmos. Environ., 62, 228–242, 2012.

615 Wang, Y., Ying, Q., Hu, J. and Zhang, H.: Spatial and temporal variations of six criteria air
616 pollutants in 31 provincial capital cities in China during 2013–2014, Environ. Int., 73,
617 413–422, 2014.
618 Lin, J., & Li, J. Spatio-temporal variability of aerosols over East China inferred by merged
619 visibility-GEOS-Chem aerosol optical depth. Atmos. Environ, 132, 111-122, 2016.
620 Liu Y, Li, Li, An, Jingyu, et al. Estimation of biogenic VOC emissions and its impact on ozone
621 formation over the Yangtze River Delta region, China[J]. Atmospheric Environment, 186
622 113–128, 2018
623 Kota, S. H., Schade, G., Estes, M., Boyer, D., & Ying, Q. (2015). Evaluation of MEGAN
624 predicted biogenic isoprene emissions at urban locations in Southeast Texas.
625 Atmospheric Environment, 110, 54-64.
626 Jiang, J., Aksoyoglu, S., Ciarelli, G., Oikonomakis, E., El-Haddad, I., Canonaco, F & Prévôt, A.
627 S. (2019). Effects of two different biogenic emission models on modelled ozone and
628 aerosol concentrations in Europe. Atmospheric Chemistry and Physics, 19(6), 3747-3768.
629 Hogrefe, C., Isukapalli, S. S., Tang, X., Georgopoulos, P. G., He, S., Zalewsky, E. E & Sistla, G.
630 (2011). Impact of biogenic emission uncertainties on the simulated response of ozone and
631 fine particulate matter to anthropogenic emission reductions. Journal of the Air & Waste
632 Management Association, 61(1), 92-108.
633 Wang, P., Ying, Q., Zhang, H., Hu, J., Lin, Y., & Mao, H. (2018). Source apportionment of
634 secondary organic aerosol in China using a regional source-oriented chemical transport
635 model and two emission inventories. Environmental Pollution, 237, 756-766.
636 Wang, L., Jang, C., Zhang, Y., Wang, K., Zhang, Q., Streets, D., Fu, J., Lei, Y., Schreifels, J., He,
637 K., Hao, J., Lam, Y.-F., Lin, J., Meskhidze, N., Voorhees, S., Evarts, D., and Phillips, S.:

638 Assessment of air quality benefits from national air pollution control policies in China.
639 Part I: Background, emission scenarios and evaluation of meteorological predictions,
640 Atmos. Environ., 44, 3442–3448, 2010.
641 Wang, Y., Ying, Q., Hu, J. and Zhang, H.: Spatial and temporal variations of six criteria air
642 pollutants in 31 provincial capital cities in China during 2013–2014, Environ. Int., 73,
643 413–422, 2014.
644 Zhang, H., Li, J., Ying, Q., Yu, J. Z., Wu, D., Cheng, Y., He, K., and Jiang, J.: Source
645 apportionment of PM2:5 nitrate and sulfate in China using a source-oriented chemical
646 transport model, Atmos. Environ., 62, 228–242, 2012.
647 Hu, J., Chen, J., Ying, Q., & Zhang, H. (2016). One-year simulation of ozone and particulate
648 matter in China using WRF/CMAQ modeling system. Atmos. Chem. Phys., 16(16),
649 10333-10350.

650 **Figure captions**

651 **Fig. 1.** Simulation domain

652 **Fig. 2.** Seasonal spatial distribution of the LAI in the model domain

653 **Fig. 3.** Seasonal distributions of the proportions of PFTs in the model domain

654 **Fig. 4.** Annual emissions of isoprene, terpene, other VOCs and total BVOCs in 2017

655 **Fig. 5.** Monthly BVOC (four types) emissions in China in 2017

656 **Fig. 6.** Seasonal emissions of isoprene, terpene, other VOCs and total BVOCs in 2017

657 **Fig. 7.** Observed and simulated monthly average of the daily 1-h maximum O_3 concentrations
658 ((Base case: anthropogenic emissions+biogenic emissions; NB case: only anthropogenic
659 emissions; NA case: only biogenic emissions, μg m^{-3})

660 **Fig. 8.** Relative difference between the surface O_3 averaged in July with and without biogenic
661 emissions (monthly average of the daily 1-h maximum, μg m^{-3})

662 **Fig. 9.** Spatial distribution of SOA simulations in July 2017 (Base case: anthropogenic
663 emissions+biogenic emissions; NB case: only anthropogenic emissions; NA case: only biogenic
664 emissions)

665 **Fig. 10.** Relative difference between the SOA concentrations averaged in July with and without
666 biogenic emissions (μg m^{-3})

667 **Figures**

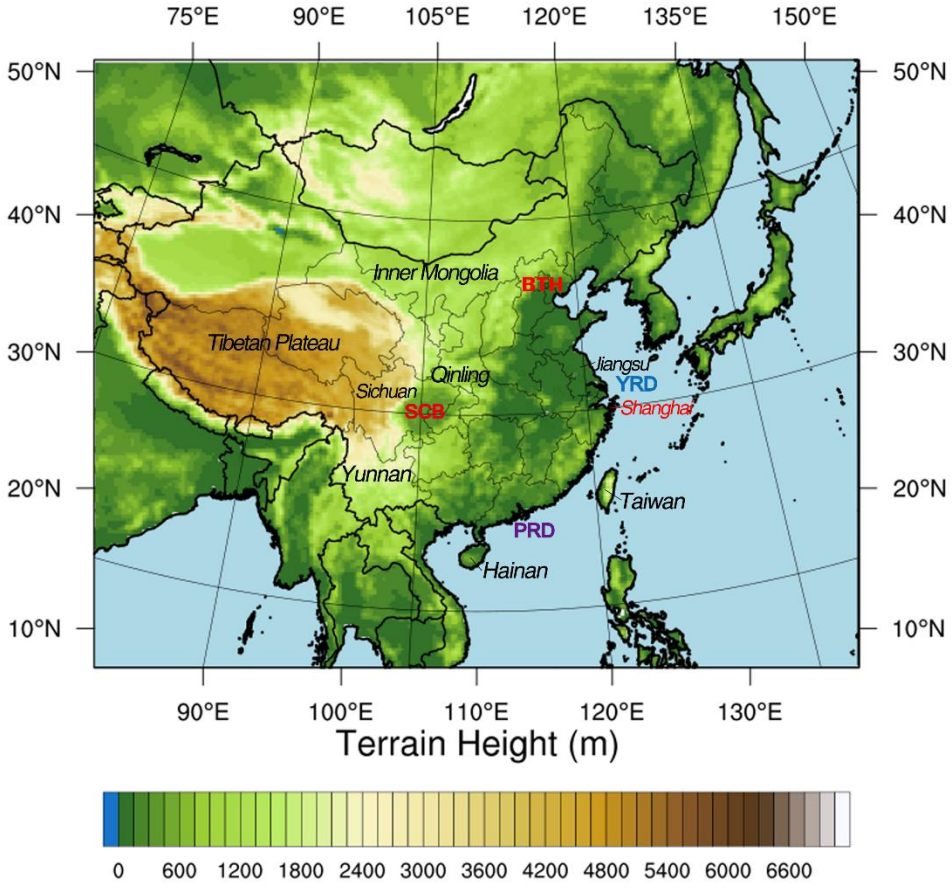

668
669 **Fig. 1**

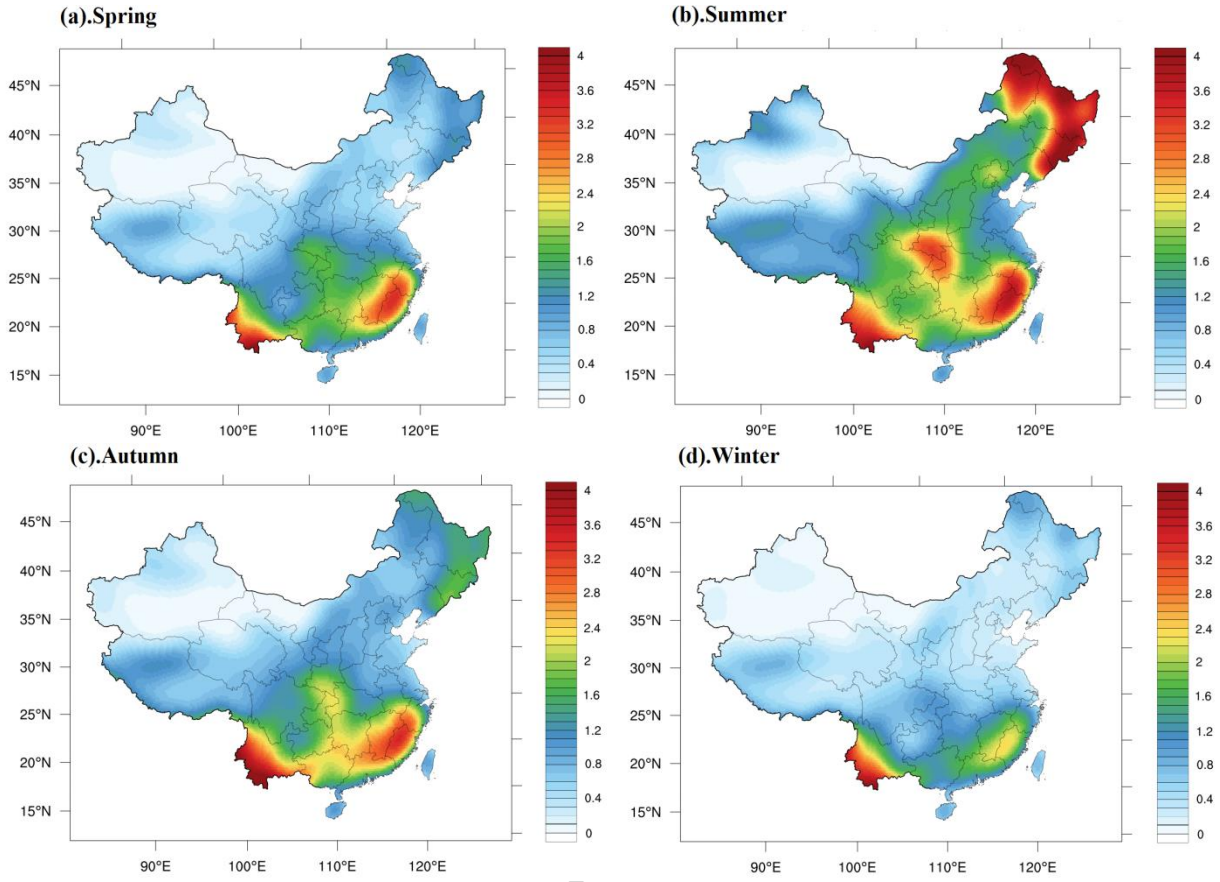

670

671

672 **Fig. 2**

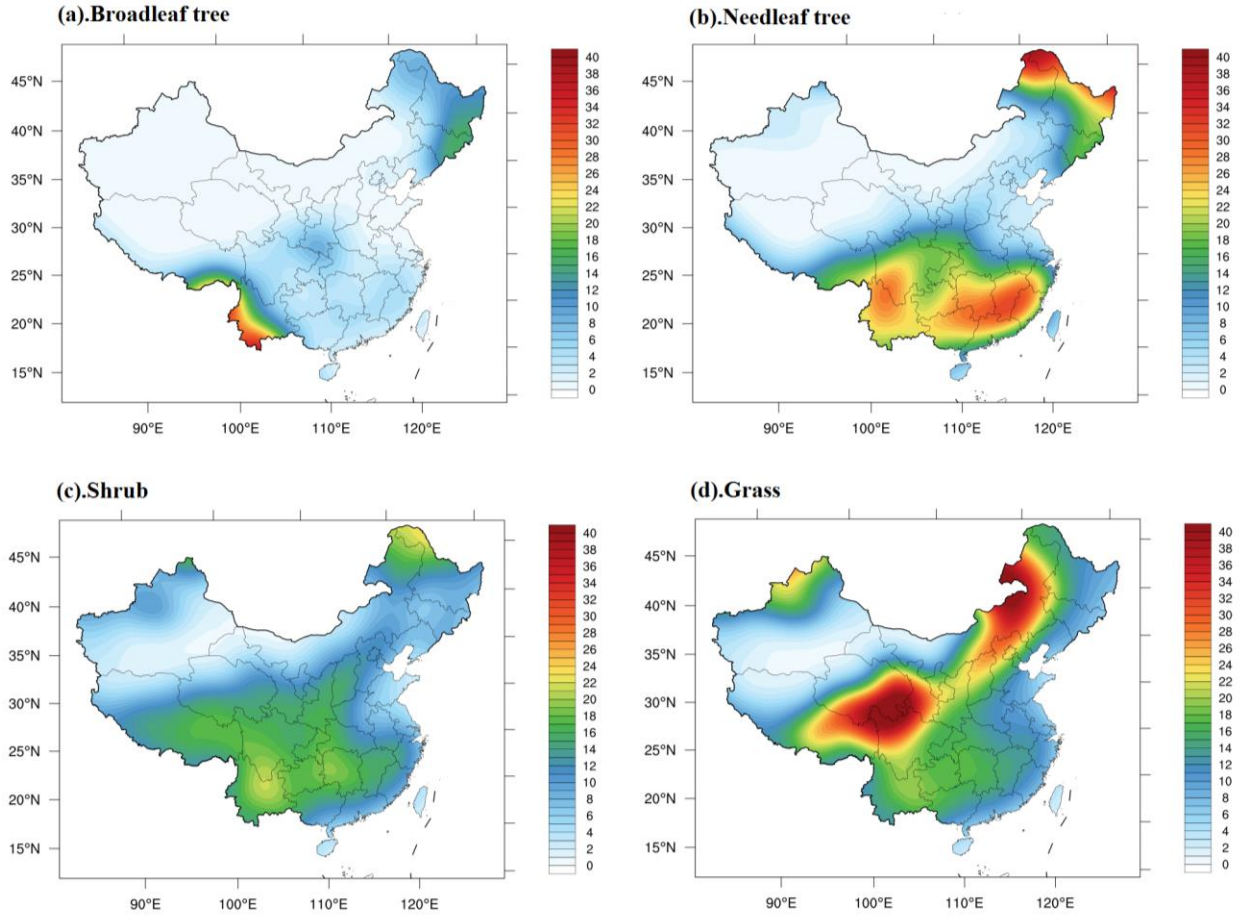

673
674 **Fig. 3**

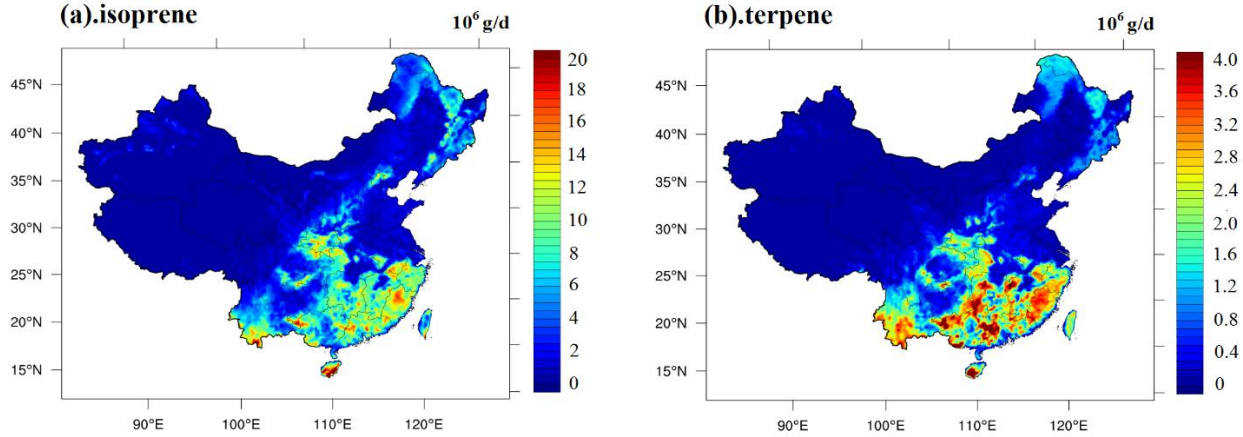

675

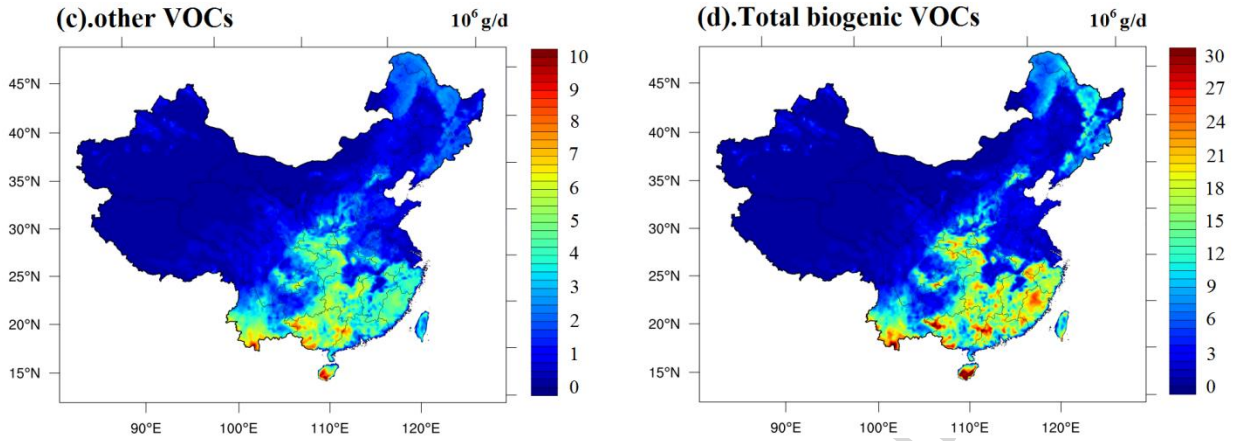

Fig. 4

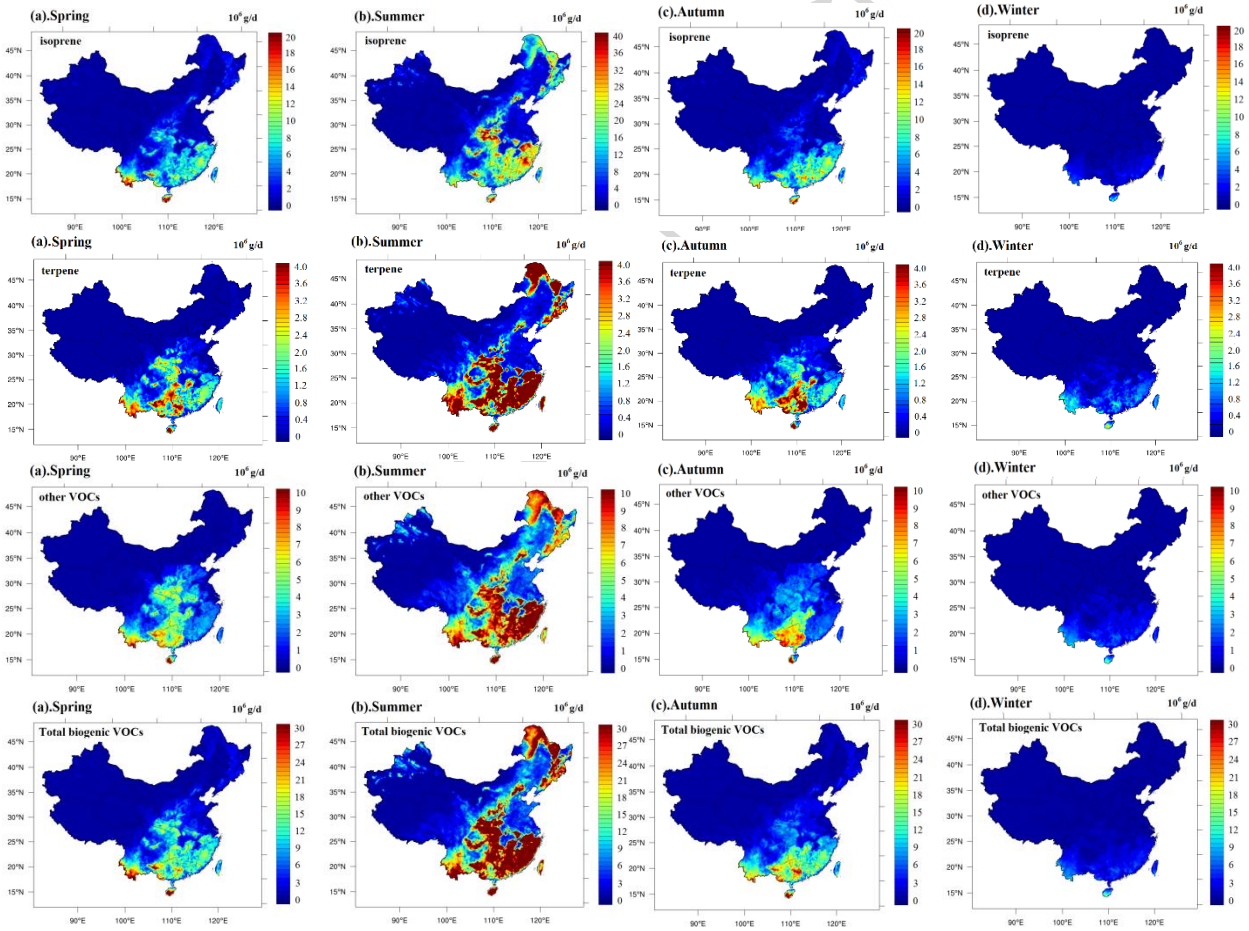

Fig. 5

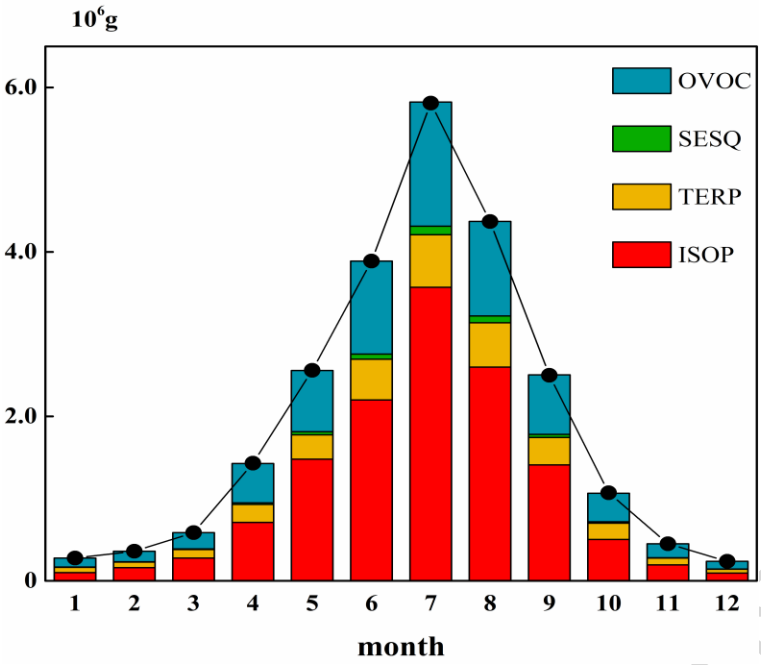

683
684 **Fig. 6**

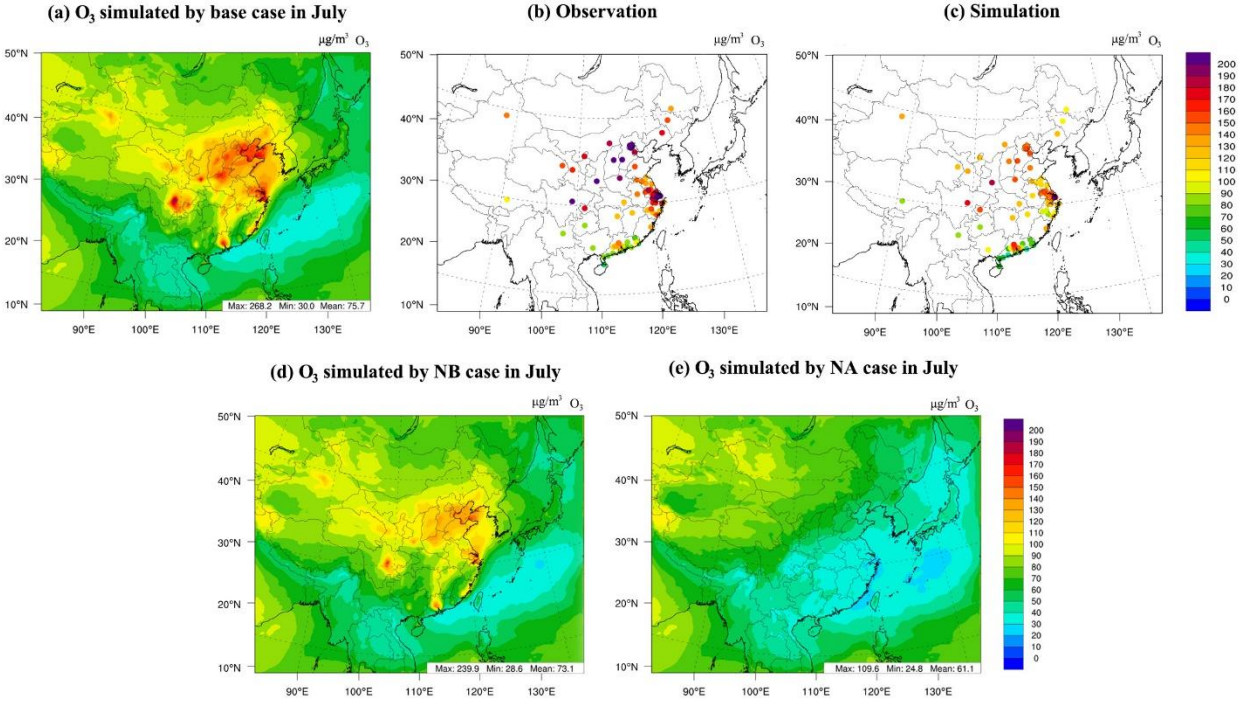

685
686 **Fig. 7**

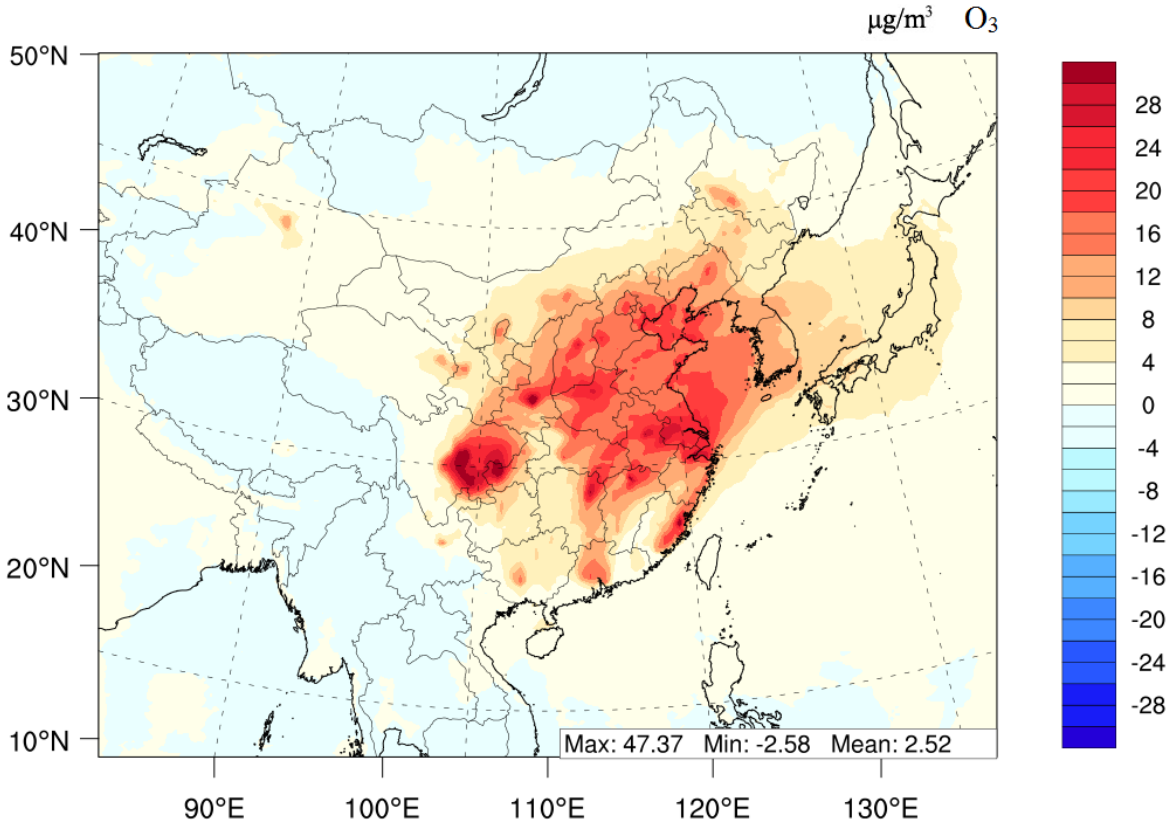

687
688 **Fig. 8**

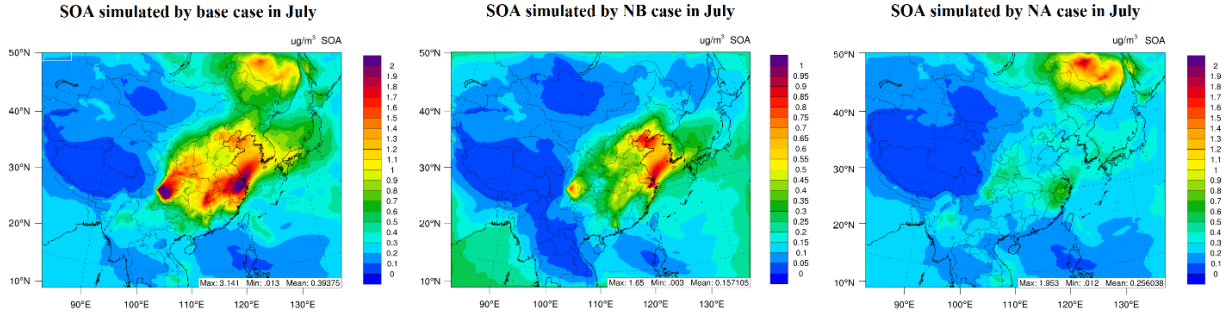

689
690 **Fig. 9**

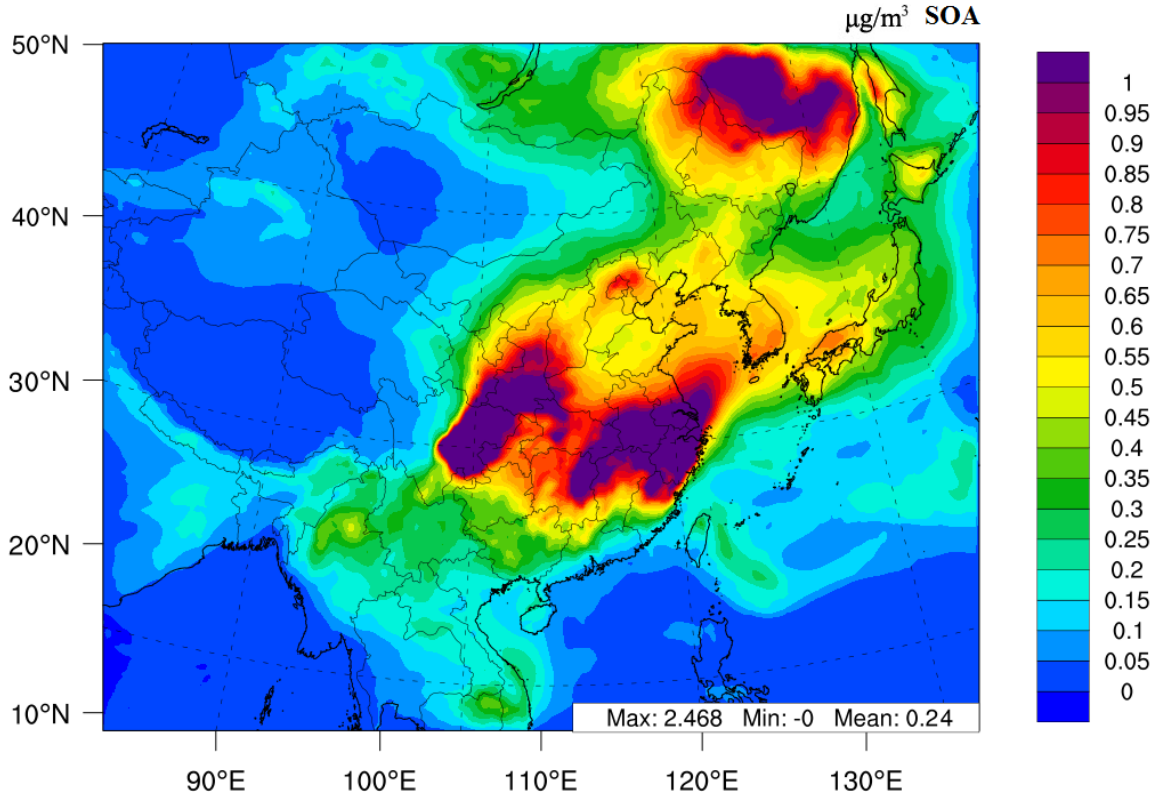

691
692 **Fig. 10**

693 ## Highlights:

694 • BVOC emissions in China were estimated at high spatial resolution by MEGAN in 2017.
695 • The impact of BVOC emissions on O_3 and SOA in China was analyzed by WRF-CMAQ
696 model.
697 • BVOC emissions were 23.54 Tg with a peak in summer and decreasing going north.
698 • BVOC emissions significantly increased surface O_3 and SOA concentrations in China.
699 • Controlling anthropogenic emissions would reduce both ASOA and BSOA.